

Towards Automatically Controlled Dosing for Selective Laser Trabeculoplasty

Katharina Bliedtner¹, Eric Seifert¹, and Ralf Brinkmann^{1,2}

¹ Medical Laser Center Lübeck, Lübeck, Germany

² Institute of Biomedical Optics, University of Lübeck, Lübeck, Germany

Correspondence: Katharina Bliedtner, Medical Laser Center Lübeck, Peter-Monnik-Weg 4, 23562 Lübeck, Germany. e-mail: bliedtner@mll.uni-luebeck.de

Received: 27 May 2019

Accepted: 9 September 2019

Published: 2 December 2019

Keywords: ophthalmology; ophthalmic optics and device; selective laser trabeculoplasty; dosimetry; micro bubble detection

Citation: Bliedtner K, Seifert E, Brinkmann R. Towards automatically controlled dosing for selective laser trabeculoplasty. *Trans Vis Sci Tech.* 2019;8(6):24, <https://doi.org/10.1167/tvst.8.6.24>
Copyright 2019 The Authors

Purpose: Selective laser trabeculoplasty (SLT) is a treatment option for open-angle glaucoma; however, it lacks an instant evidence for successful irradiation. So far ophthalmologists use the visible appearance of permanent champagnelike bubbles (macro bubbles) as an indicator for appropriate pulse energy. We hypothesize that micro bubbles, which start energetically far below the appearance of macro bubbles, already trigger the therapeutic benefit. Here we present two methods to capture the onset of these micro bubbles.

Methods: The trabecular meshwork of freshly enucleated porcine eye globes was irradiated with a series of 15 pulses with a pulse duration of 1.7 μs and with increasing energy at a repetition rate of 100 Hz per each spot of 200 μm in diameter. An optical and an optoacoustic method have been developed and appropriate algorithms investigated towards the real-time detection of the onset of micro bubbles.

Results: Both observation methods are capable of detecting micro bubble nucleation. Threshold radiant exposures were found at $310 \pm 137 \text{ mJ/cm}^2$. By combination of both methods a sensitivity and specificity of 0.96 was reached.

Conclusions: In case that the therapeutically demanded pressure reduction is already achieved with these micro bubbles, which needs to be proven clinically, then the methods presented here can be used in an automatic feedback loop controlling the laser irradiation. This will unburden the clinicians from any dosing during SLT.

Translational Relevance: Automatic real-time pulse energy dosing based on the formation of micro bubbles in SLT significantly improves and facilitates the treatment for the physician.

Introduction

Glaucoma is a multifactorial disease where an elevated intraocular pressure (IOP) is considered a major risk factor to cause damage to the optic nerve. The first-line treatment to lower the IOP and prevent optic nerve damage is typically eye drops.¹ Administration of eye drops requires high compliance of patients; treatment adherence of patients with chronic disease is reported to be approximately 75% in general.² Nevertheless, good adherence for one daily glaucoma medication was reported, but adherence drops for patients with complex dosing regimens.³ A high number of dosing errors was reported,³ as well as a poor success rate of proper instillation of eye drops.⁴ In 1979, Wise and Witter⁵ reported an IOP

lowering using an argon laser applying 100 burns at 1 to 1.5 W using a pulse duration of 0.1 seconds and a beam diameter of 50 μm . Argon laser trabeculoplasty (ALT) showed an equivalent IOP control compared with trabeculectomy, but with fewer complications.⁶ The laser treatment causes coagulative damage to the trabecular meshwork (TM). The tissue shrinkage around the coagulation sites likely causes an opening of adjacent tissue, which results in an increased outflow,⁶ thus one mechanism of ALT is believed to be thermo-mechanical.

Selective laser trabeculoplasty (SLT) was initially described by Latina and Park⁷ in 1995. SLT uses a frequency-doubled Q-switched Nd:YAG laser at 532 nm with a pulse duration of 3 ns and a spot size of 400 μm , which covers the entire anteroposterior height of

the TM.^{8,9} In contrast to ALT, SLT showed no coagulative damage and structural change in the TM, which makes SLT a safer and repeatable procedure with effective IOP reduction.¹⁰ It has been demonstrated that SLT selectively targets the pigmented TM cells without damaging adjacent cells.⁷ The exact mechanism of IOP reduction is not fully understood yet, but biological changes on a cellular level after laser treatment are proposed to initiate an increased outflow because no morphological changes were found.¹⁰ Among these biological effects changes in the gene expression, cytokine secretion, matrix metalloproteinase induction, increased cell division, repopulation of damaged areas, and macrophage recruitment have been reported.¹¹

There is no standardized protocol for SLT. A variation of the number of applied spots from 50 to 100, as well as a variance of the treated area from 180° to 360° can be found in the literature.¹² Nagar et al.¹³ compared 90°, 180°, and 380° SLT with medication and found that 180° and 360° is effective, whereas 90° SLT is not. The difference in effectiveness between 180° and 360° is not significant. Also, the energy level per spot and the total delivered energy is not fixed. In their initial study, Latina et al.⁸ proposed to set the energy to 0.8 mJ and decrease the energy in 0.1 mJ steps until no visible effect or bubble formation (champagnelike bubbles [CBs]) was observed. The treatment was then performed at this energy level, and each spot was monitored to adjust the energy if bubble formation occurs again. Laser energies per spot between 0.6 and 1.2 mJ are used,¹² and the expected endpoint is no visible effect nor small bubbles.

The optimal energy setting has been investigated. It was shown that lower energy SLT (0.3–0.5 mJ over 360°, half of conventional laser energy) has the same IOP lowering effect compared with conventional energy SLT with fewer side effects.¹⁴ In contrast, another study found that a higher total energy (214.6–234.9 mJ compared with 100 mJ) seems to be associated with an improved IOP lowering effect, but this study had a small sample size and a short follow-up period.¹⁵ The optimal dosage and endpoint of SLT, as well as the therapeutic window, seems to be still debatable.

The definition of a suitable detectable endpoint and an automatic, objective monitoring when each spot reaches this endpoint could help to reduce overtreatment and undertreatment, would make the treatment more reliable, and reduce the treatment time. We hypothesize that such an endpoint could be based on the formation and observation of micro

bubbles (MBs), which are most likely the cause of cell death and take place far below the threshold for the formation of champagnelike macro bubbles.

The ophthalmoscopically visible CBs that are used to initially titrate the energy are stable gas bubbles that evolve from small vaporization bubbles when the radiant exposure is large enough. Initial MBs are the result of fluid vaporization at the surface of the TM-melanosomes after their rapid heating to a sufficient temperature.¹⁶ The size of these MB is in the scale of 10 to 20 μm. Micro bubble formation (MBF) seems to be the origin of cell death^{16,17}: because of the almost simultaneous formation of these transient MBs around all melanosomes in the irradiated cell, the cell volumes increase and the cell structures are mechanically disrupted.

Lin¹⁶ reported that stable macroscopic gas bubbles could be observed after the collapse of MB when the radiant exposure is increased approximately 10 times above the threshold for cavitation. So, it seems that the current endpoint used for SLT is far above the threshold for selective cell killing. In the case of SLT, a slightly higher energy is not as critical as, for example, compared with selective damage of the retinal pigment epithelium (RPE) in selective retina therapy (SRT) where the adjacent neuronal retina needs to be spared. But not only overtreatment is problematic, also undertreatment is highly possible, because there is no visible endpoint and no indication for a successful treatment.

In SRT, MB can be detected successfully when selectively targeting the RPE using different optical^{18–20} and acoustical²¹ techniques. The formation of MBs itself or a displacement of other scatterers will on the one hand change the light scattering characteristics. On the other hand, pressure waves will be emitted during the formation and dynamics of MB. The change in the scattering characteristics can be detected when analyzing the backscattered pulse. Without MBF, the temporal shape of the backscattered pulse will be almost identical to the applied pulse. The change in scattering properties caused by MB will add a high frequency “modulation” to the backscattered temporal pulse shape. Further, short pulses used in SRT and SLT will cause optoacoustic (OA) pressure waves because of the thermoelastic expansion of the absorbing medium. The expansion and collapse of MB lead to additional pressure waves that can be differentiated from the thermoelastic expansion.²¹

The aim of this work is to investigate an optical and optoacoustical monitoring during microsecond-SLT ex vivo in porcine eye globes. Both methods are

Table 1. A Comparison of the Parameters Used in Conventional SLT and Microsecond-SLT

	Conventional SLT	μ s-SLT	
		Single Pulse	Pulse Train ^a
Pulse duration, ns	3		1700
Spot diameter, μ m	400		200
Pulse energy, mJ	0.6–1.2	0.03–0.35	0.38–3.94
Radiant exposure, mJ/cm ²	477–955	96–1114	1074–12,533

^a Pulse train of 15 pulses with linearly increasing energy, with the minimum energy being half the energy of the maximum energy, set in the system.

adapted from SRT. In contrast to conventional SLT where one 3 ns pulse per spot is applied, here a series of 15 pulses with a pulse duration of 1.7 μ s is used. Despite the increased pulse duration, the pulse energies used in this study are in the same range or even below the typical pulse energies used in conventional SLT (see Table 1). In this work, signal changes shall be identified that can be associated with MBF. Sensitivity and specificity for detection algorithms shall be determined as well as threshold radiant exposure for MBF.

Material and Methods

Setup

The system used in this work is the R:GEN (Lutronic Corp., Goyang-si, Republic of Korea). It consists of a frequency doubled Q-switched Nd:YLF laser (527 nm), applying a series of 15 pulses with a pulse duration of 1.7 μ s with stepwise increasing energy at a repetition rate of 100 Hz. The maximum energy can be set between 30 and 350 μ J, and the system will apply a linear energy ramp starting at half of the maximum energy. Table 1 summarizes the parameters typically used in conventional SLT in comparison with those used in this approach.

The laser radiation is coupled to the integrated slit lamp by a multimode fiber (numerical aperture [NA] = 0.11 and core diameter of 50 μ m). The chosen magnification of 4 results in a fixed spot size of 200 μ m in air. There are intensity fluctuations overlaying the top hat beam profile, and the intensity modulation factor (IMF) defined as the peak-to-mean intensity ratio was measured to be 4.1. The laser light is applied to the chamber angle of the enucleated porcine eye by a modified gonio contact lens.

Two different detection methods are included in the setup, which allow recording of backscattered light and OA transients during the application of laser

pulses, which are used to correlate signal changes to the formation of MB.

Both algorithms described below are independent of the algorithm implemented in R:GEN for SRT. The R:GEN algorithms are neither used nor considered in this study at any time.

Optical Detection

The light that is backscattered from the TM is split from the treatment light path by an 80:20 beam splitter before it passes a 1-mm aperture, regulating stray light, speckle properties, and irradiance. After the aperture, the backscattered light is coupled into a fiber and guided to an avalanche diode. Diode signals are amplified within the R:GEN system and then digitized externally to the R:GEN system using a NI PXIe-5122 (National Instruments, Austin, TX) digitizer card with a sampling frequency of 100 MS/s and a resolution of 14 bit.

OA Detection

A gonioscopic contact lens with a mirror is usually used to visualize the chamber angle. In order to record OA transients, an Ocular Latina 5 Bar Indexing SLT contact lens (Ocular Instruments Inc., Bellevue, WA) was modified. An opening is faced opposite to the mirror, as can be seen in Figure 1. In a multiple step gluing process, a half moon-shaped piezoelectric transducer with a diameter of 19 mm, a height of 6 mm, and a resonance frequency of 1 MHz is placed in the contact lens. The position of the transducer allows sufficient closeness to the ultrasonic source in the chamber angle without obstructing the light path and the view through the gonioscopic lens. The pressure waves travel through the chamber angle and the contact lens before they reach the transducer. The recorded signal is amplified (44 dB) by a charge amplifier (Panametrics 5662 Ultrasonic PreAmp, Olympus, Hamburg, Germany) and digitized using the same oscilloscope card as for the diode signal. Besides the acquired optical and acoustic raw data,

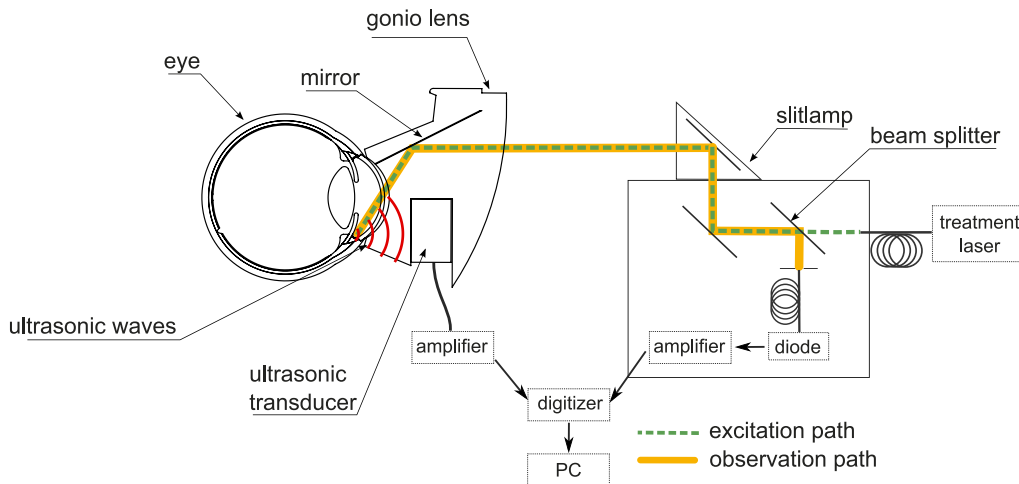


Figure 1. Schematic drawing of the setup together with the modified contact lens with included transducer.

which are stored on hard disk, the R:GEN provides meta data as pulse energy or pulse number for every pulse, which is stored as well.

Ex Vivo Experiments and Classification

Seven hundred forty-three spots were applied in 44 freshly enucleated porcine eye globes. Eyes were used within 3 hours after enucleation and placed in a special mount in front of the slit lamp together with the contact lens. Methocel (2%) was used for index matching. The appearance of CB was observed by the experimenter for each spot through the slit lamp using the white slit light during and after irradiation and documented for each spot. However, there is no visible observation for MBF that can be used as a

reference to evaluate the performance of the detection methods. Also, other imaging modalities, live dead assay, histology, or OCT were not found to be suitable in this study to identify cell damage for each applied spot. Because two independent signal types were recorded simultaneously, one can be used as a reference for MBF in the second. Therefore, the backscattered light of each pulse of each spot was classified manually. The optical raw data are used rather than the acoustical because signal changes are easier to be recognized on each single pulse. Example data for the manual classification can be seen in [Figure 2b](#). Three example pulses are plotted over time, which are the first (blue), 8 (red), and 15 (yellow) pulses of a burst (also represented in [Fig. 2a](#)).

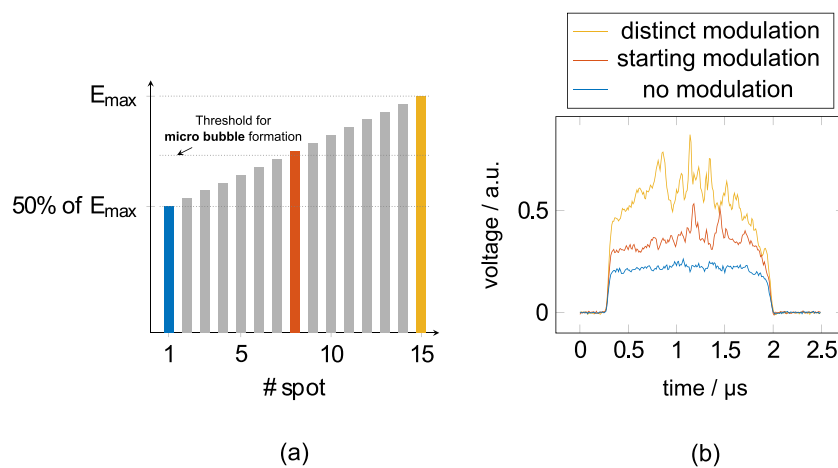


Figure 2. (a) Fifteen pulses are applied where the first (blue) one has 50% of the maximum energy that is applied with the last pulse (yellow). The maximum energy can be adjusted in the laser system. (b) Example of optical raw data from pulse one; 8 and 15 are plotted. The first (blue) pulse has a smooth shape similar to the applied pulse and is categorized as no modulation. The 8 (red) and 15 (yellow) pulses are superimposed by high-frequency signal components and categorized as modulation.

The first (blue) pulse has a smooth shape and is identical to the laser pulse shape from the R:GEN. The alterations are in the same magnitude as the noise in front and behind the pulse. A pulse with this shape is categorized as “no modulation.” However, the red and yellow pulse show high-frequency signal components on top of the pulse and are therefore classified as “modulation.” Those modulations were associated with the appearance of MB in other studies¹⁸ and are also considered a suitable reference in this study. If no distinct decision can be made, the pulse is categorized as “unknown.” Pulses categorized as unknown usually show one or two small peaks only slightly larger than the noise. This manual classification is used as gold standard for performance evaluation of the detection algorithms in this work.

Detection Algorithms

Optical

High frequency modulation around several MHz are used as an indicator for MBF, and the following algorithm is calculating the amount of modulation represented by the reflectometry (RM) value of each pulse. The algorithm is similar to the one used in SRT with a detailed explanation by Seifert et al.¹⁸ The main algorithm includes two parts: first a signal validation and then a feature extraction. The validation part ensures sufficient signal-to-noise ratio (SNR; the maximum signal value needs to be a factor 2.5 larger than the mean noise) and detects saturation (more than 50 consecutive samples reach the saturation limit of 3.5 arbitrary unit [a.u.]). The most relevant processing steps that are necessary to extract the high frequency modulations from the laser pulse are illustrated in the following:

1. The offset is removed.
2. Each detected pulse is normalized to the area under the curve.
3. The jitter is removed ensuring that all 15 pulses start at the same time.
4. The features are then extracted with a bandpass filter (Butterworth type) with a lower cutoff frequency of 7 MHz, an upper cutoff frequency of 35 MHz, and an order of 3.
5. The filtered data are squared and are referred to as $R_F(t)$.
6. To remove the filter artifacts at the beginning and the end of the signal, a region of interest with the start point $t_S = 0.6 \mu\text{s}$ and the endpoint $t_E = 1.6 \mu\text{s}$ is defined. Within this region of interest, all values that are above the threshold

R_{th} are summed up. R_{th} is defined as product of the mean noise before the pulse and a threshold factor set to 50.

This results in a one-dimensional value, here called RM-value, for each single pulse, which represents the amount of MB-induced modulations:

$$RM = \sum_{t=t_S}^{t_E} R_F(t) \text{ for all } R_F(t) \geq R_{th} . \quad (1)$$

Optoacoustics

In contrast to the optical method, it is difficult to differentiate between MB and thermoelastic expansion using only one transient of one specific pulse. Rather one would have to compare each transient, for example, with the first transient of each spot. In this way, it is possible to find a nonlinear amplitude change or shifts between transients. First, a validation test is performed before applying the algorithms to the signals. Signals that are saturated (more than 50 consecutive samples reach the saturation limit of 2.5 a.u.) or have insufficient SNR (the maximum signal value needs to be a factor 1.6 larger than the mean noise) are excluded from the evaluation. In addition, all 15 pulses of one spot are excluded when the SNR of the first transient is too low, because it serves as a reference.

The following algorithm steps are performed to identify the pulse-to-pulse change:

1. The offset is removed.
2. A bandpass filter (lower cutoff frequencies of 10 kHz, upper cutoff frequency of 200 kHz, and an order of 4) is used to remove noise.
3. A region of interest with the start point $t_S = 15 \mu\text{s}$ and the endpoint $t_E = 100 \mu\text{s}$ is used to extract a part of the signal. At $t = 0$ the laser pulse starts.
4. Using the measured transient data of the first pulse $T_1^M(t)$ with its energy E_1 and the measured energy of each pulse E_k , a theoretical transient $T_k^T(t)$ can be calculated for each pulse:

$$T_k^T(t) = \frac{T_1^M(t)}{E_1} E_k, \quad (2)$$

where $T_k^T(t)$ has the shape of the initial transient scaled by the energy increase. This is the theoretical transient one would expect if only thermal expansion is causing the pressure waves, because the thermal expansion scales proportionally with the applied energy in first order. The difference of the theoretical transient $T_k^T(t)$

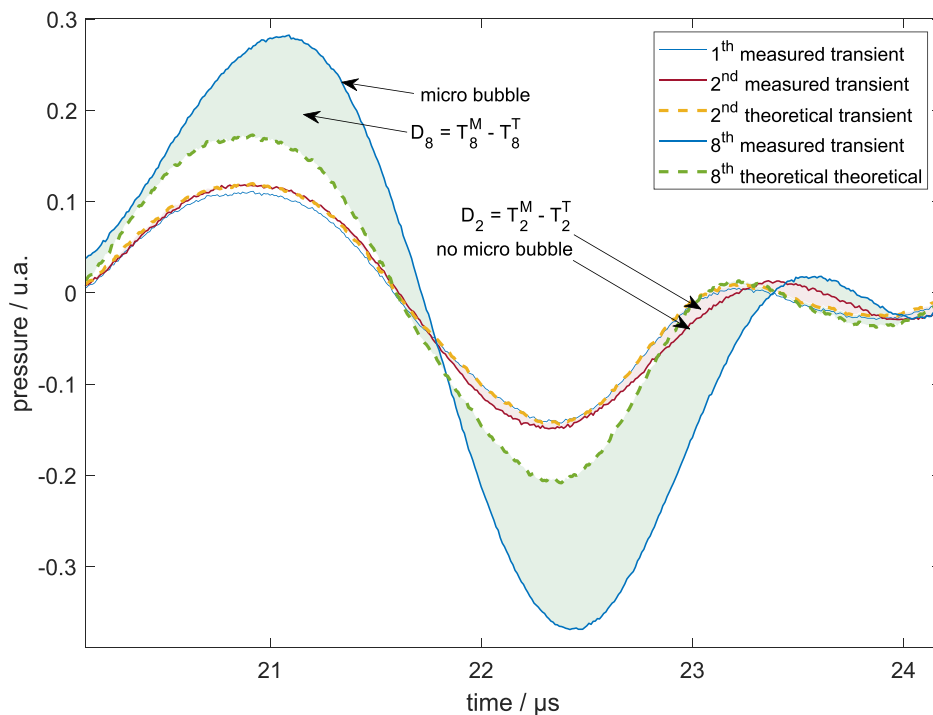


Figure 3. Preprocessed example transients (offset removed and filtered) for one pulse below (red) and above (blue) the threshold for MBF. The colored area represents the difference of each pulse to its theoretical pulse that would arise from thermoelastic expansion alone.

and the actual measured transient $T_k^M(t)$ can then be used as a measure for the existence of MB. Figure 3 shows that the difference of a pulse above MB threshold to its theoretical pulse is larger than the difference of a pulse below MB threshold. The transient of the subthreshold pulse almost matches its theoretical pulse. From the difference, a one-dimensional OA value is calculated:

$$OA_k = \sum_{t=t_S}^{t_E} |T_k^M(t) - T_k^T(t)|. \quad (3)$$

For both, the acoustic and optic detection method, algorithms are designed to quantify the presence of MB that are represented by a one-dimensional value for both methods. Here, the algorithm parameters are manually adjusted in order to maximize the combination of sensitivity and specificity, that is, the Youden index. A receiver operating characteristic (ROC) analysis is used to find the best Youden index, and the corresponding RM and OA values represent the best threshold to separate the modulation from the no modulation category.

Results

Data Set Overview

A total number of 743 spots were applied. The measured energy of the last pulse of each spot range from 25.9 to 340 μJ . The distribution of the maximum energy of each spot is illustrated in Figure 4 on the left alongside with the histogram of the energy of all 11,145 pulses on the right.

In 24.4% of all spots, CBs were observed through the slit lamp during irradiation. They are displayed as red bars in the histogram in Figure 4.

Following the manual categorization process, 60.8% of all pulses are categorized as modulation, 34.0% as no modulation, and 5.2% could not be categorized as either of those and were labeled unknown. The energy distribution of all three categories is plotted in Figure 4 in the right. Energy for MBF range from 23.1 to 340 μJ .

CB Observations

During the application of 181 spots, CBs were observed through the slit lamp. The maximum energy of these spots range from 117.8 to 334 μJ . In 95% of

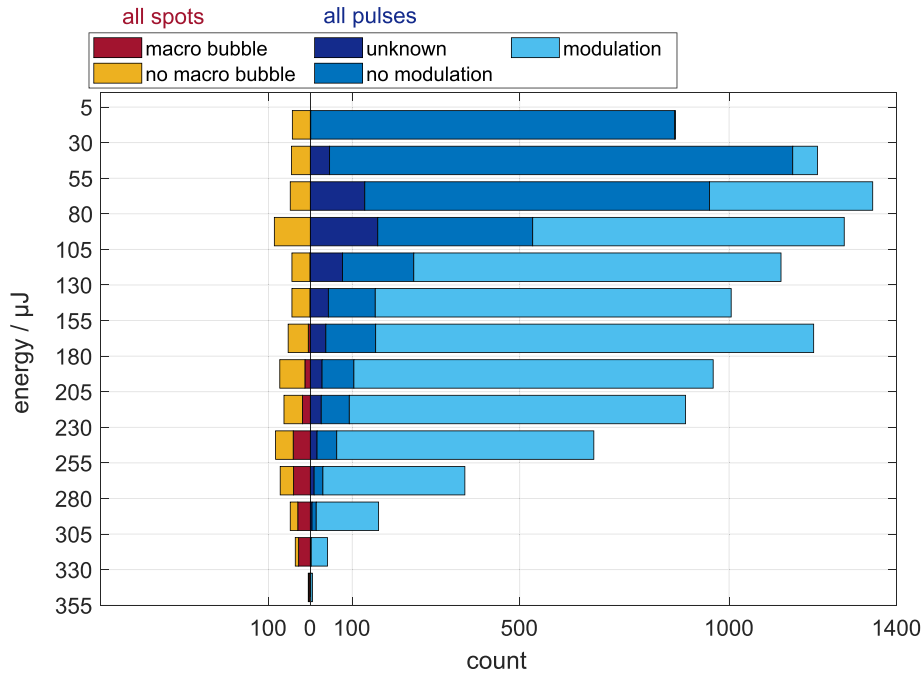


Figure 4. Histogram of the maximum set energy of each spot alongside with the pulse energy of all pulses. Spots where CBs were observed are displayed in red. The different classes of the manual categorization of each pulse are color coded in different shades of blue.

these spots, the manual categorization of all 15 pulses is modulation, and it is not possible to identify the exact pulse that causes the formation of CB. However, in nine spots, at least the first pulse showed no modulation in the RM raw signal, and one more spot had at least one pulse that was not categorized as modulation but was not the first. When assuming that at least the last pulse in each spot needs to cause CB, one can calculate an energy factor needed to produce CB.

An example can be seen in Figure 5. The spot causes CB and the energy is plotted over the pulse number. The energy of the last pulse with no modulation is 160 μJ, whereas the maximum energy is 262 μJ resulting in a maximal ratio of 1.64. The mean ratio of all 10 spots is 1.76 ± 0.24 .

Optical Detection

From the total 11,145 pulses, 9980 were used for evaluation. During signal validation, 37 pulses generated a saturation error and 576 pulses a SNR error and were therefore excluded from the evaluation as well as all 552 pulses that were categorized as unknown. From the remaining pulses, 68% (6771 pulses) are in the modulation category and 32% (3209 pulses) in the no modulation category.

RM raw data examples are shown in Figure 6a. In

each plot, the first and last pulse of a spot is displayed. All red curves are in the modulation category, and all of them show distinct modulation on top of the pulse. In contrast all blue curves (no modulation) have a smooth shape; only some pulse deformation can be seen in spot 1.

Next to the raw data, the calculated RM values for each of the four spots are shown in Figure 6b. The RM values are plotted over the applied energy of every pulse. High energies do not always lead to high

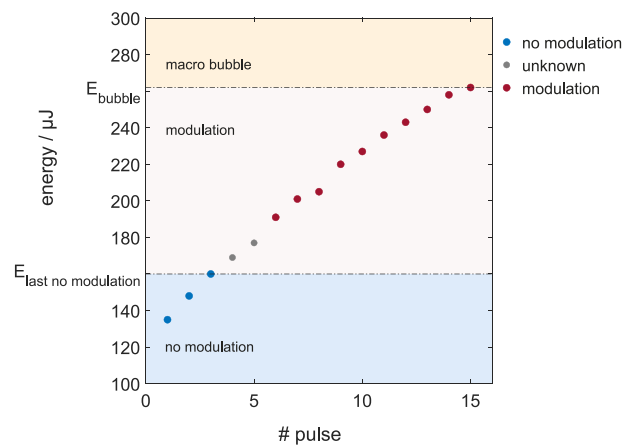


Figure 5. Energy is plotted over the pulse number of an example spot that resulted in CBs.

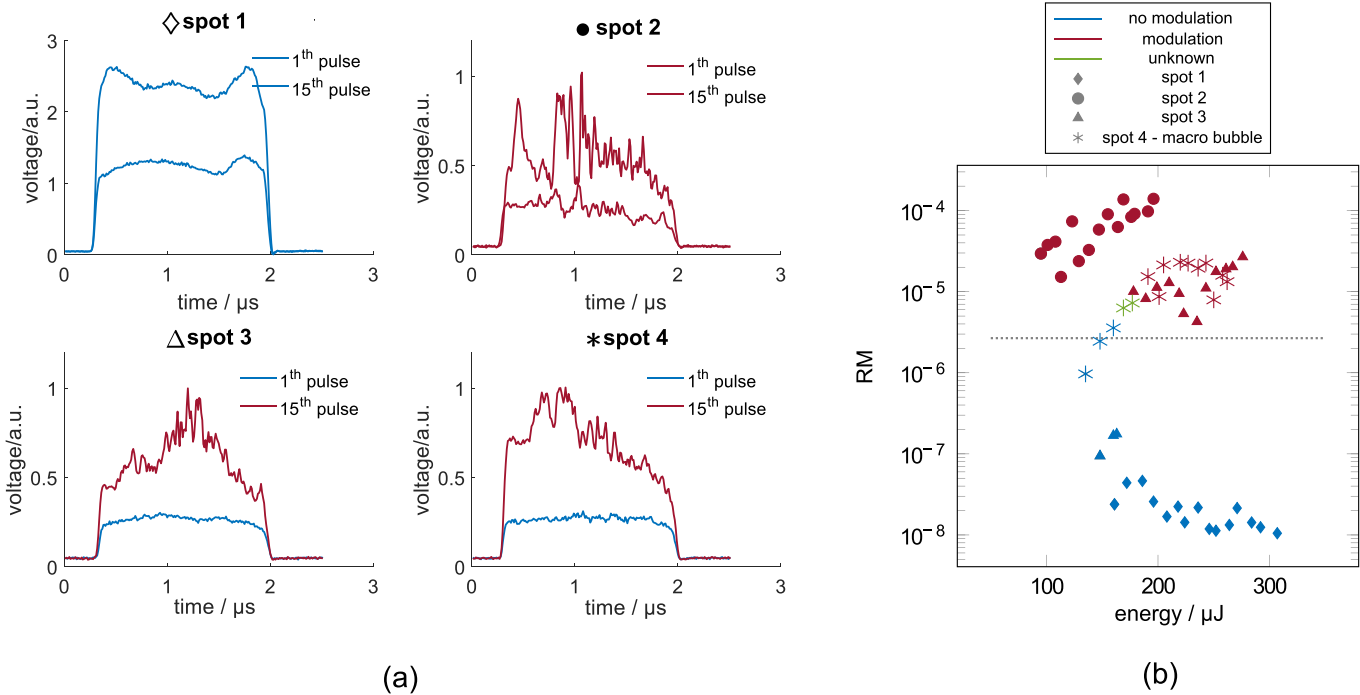


Figure 6. (a) The RM raw data of the first and last pulse of four examples are shown, respectively. *Blue* pulses belong to the no modulation category, and *red* pulses are categorized as modulations. (b) The calculated RM values of all pulses of the same four spots are plotted over the applied energy. The *dashed line* represents the best RM threshold.

RM values or MB. All pulses from spot 1 show no modulation; therefore, their RM values are small, despite their high signal amplitudes. In contrast, the pulses of spot 2 have much smaller amplitudes but large modulation, which cause high RM values. The dashed line in Figure 6b represents the calculated best RM threshold.

OA Detection

For the evaluation of the OA algorithm, only 7446 pulses could be used, which is over 2000 pulses less compared with the RM algorithm, which is a result of the validation process. All first pulses need to be excluded because they are used as reference and all have an OA value of zero (and are also not plotted in the scatter plot in Fig. 7b). Because the OA algorithm uses the first pulse as reference, all pulses of all spots need to be excluded if the first pulse causes a SNR error. This results in 1722 pulses being excluded because of a SNR error. Another 746 caused a saturation error. Only single pulses causing a saturation error are excluded, not the whole spot, because it has no influence on the calculation of OA values of all other pulses in the spot. After signal validation, an additional 488 unknown pulses were excluded. This results in 75.3% pulses in the modulation category

and 24.7% in the no modulation category. Figure 7 shows the same four example spots as Figure 6. Below MBF threshold, the amplitude of the recorded pressure transient is proportional to pulse energy as can be seen in spot 1 of Figure 7a where the OA transients after preprocessing (offset removal and filtering) are shown. The shapes of all recorded transients are similar. Also, the shape and amplitude of the transient are almost identical to the theoretical transient that can be seen in the left plot of Figure 7a. The similarity of the measured and theoretical transient result in small OA values, which are plotted in Figure 7b over the applied energy of each pulse. All transients of spot 1 are below the best OA threshold indicated by the dashed line. In contrast, almost all transients of spot 3 (Fig. 7a) show not only a different amplitude than their theoretical transients but also a different shape that indicates the formation of MB. Only the second transient seems to be similar to its theoretical one and is therefore correctly assigned as below threshold. Already the third transient shows a clear nonlinear amplitude increase and a shift to the right. This results in a higher OA, and the pulse is wrongly assigned as above threshold by the algorithm.

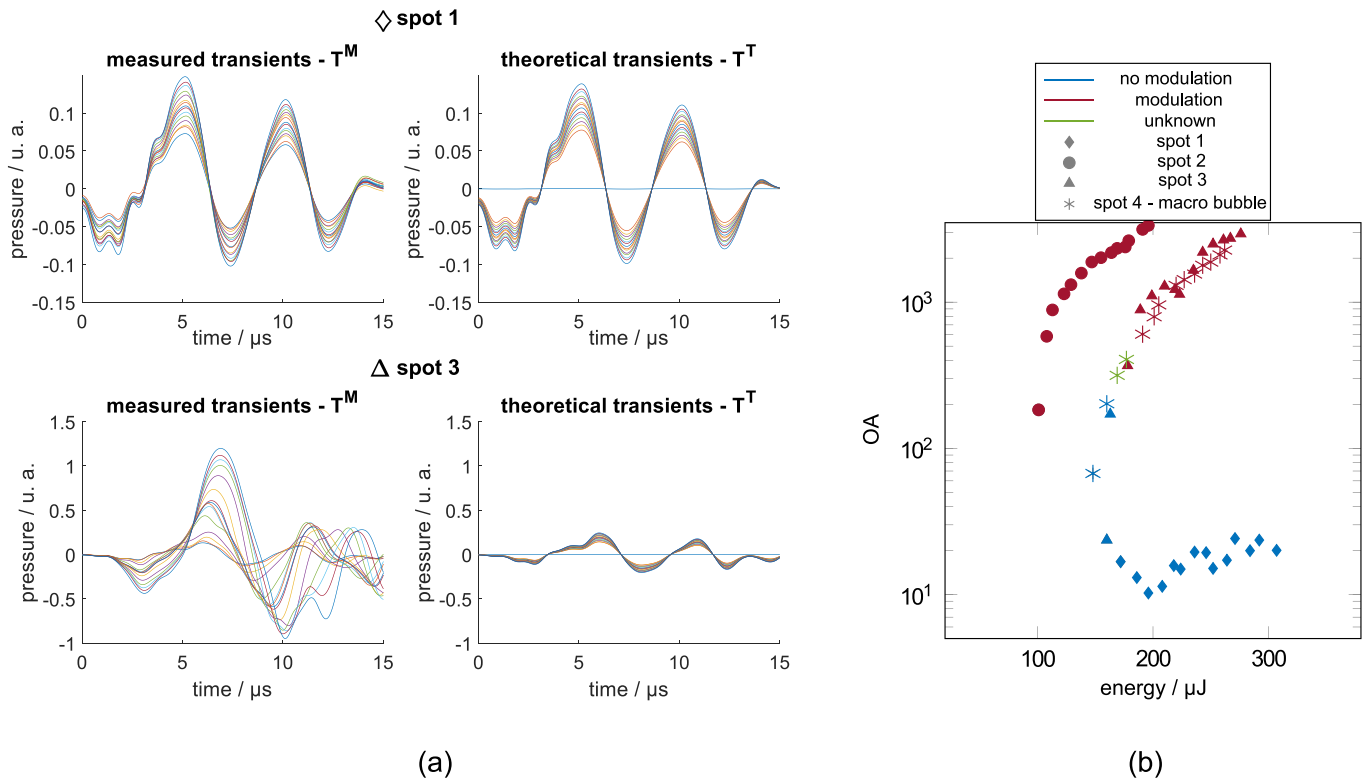


Figure 7. (a) All 15 measured and theoretical transients of two examples are shown. (b) The calculated OA values of the two spots and two more are plotted over the applied energy. The *dashed line* represents the best OA threshold. *Blue* pulses belong in the no modulation category, and *red* pulses are categorized as modulations.

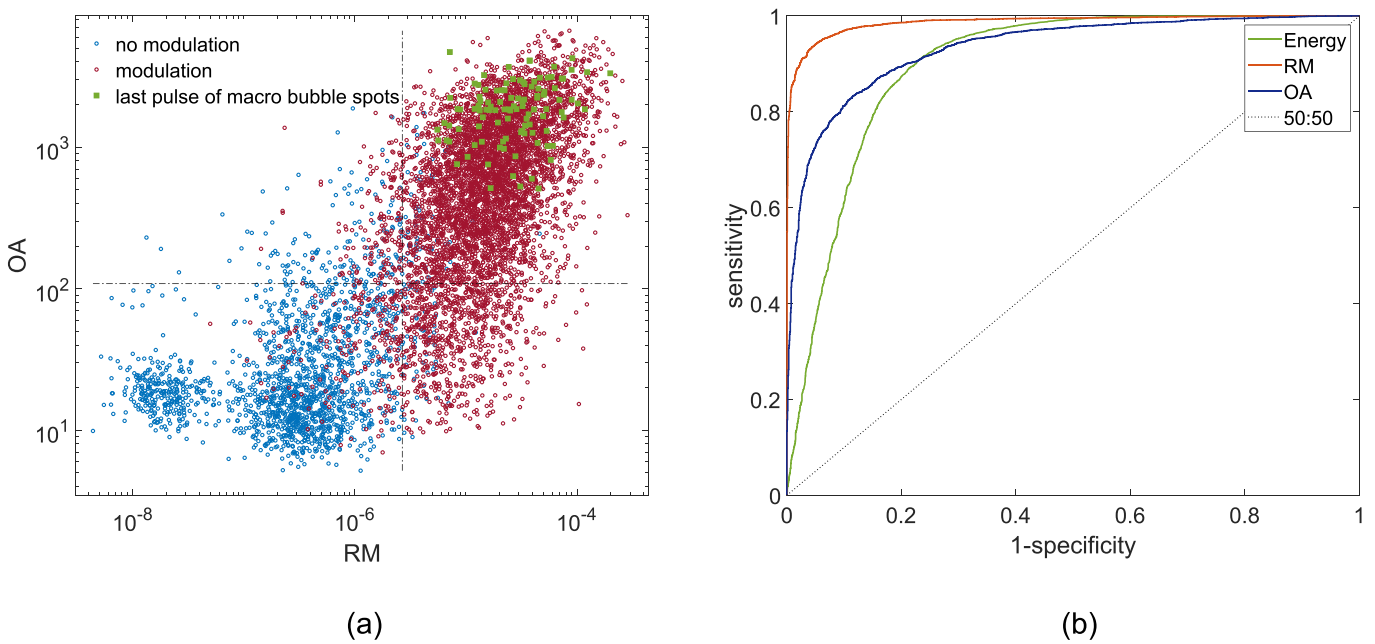


Figure 8. (a) OA values are plotted over RM values for each evaluable pulse. *Dashed lines* indicate the best threshold for each algorithm, respectively. (b) ROC plot of the pulse wise evaluation of the RM and OA algorithms together with the energy.

Table 2. Best Threshold, Sensitivity, and Specificity for Each Algorithm

Algorithm	Best Threshold	Youden Index	Sensitivity	Specificity
Energy	87.2 μ J	0.68	0.90	0.77
RM	2.67E-6	0.90	0.94	0.95
OA	108.57	0.72	0.83	0.89

Statistical Analysis and Comparison of Detection Methods

When plotting OA values over RM values of all pulses that can be evaluated by both methods as can be seen in Figure 8a, it seems that the RM algorithm has a better performance to separate both categories. In the same plot, the last pulse of spots that cause CB is plotted as well. The ROC plot of both algorithms and the energy is shown in Figure 8b. With a sensitivity of 0.94 and specificity of 0.95, the RM algorithm outperforms the energy. The OA algorithm is only slightly better compared with the energy. All values can be found in Table 2.

As a second performance measure, the accuracy of each algorithm to identify the modulation at the correct position within each spot can be evaluated. Figure 9a shows a histogram of all spots evaluated by

the RM algorithm. The green bar on the left represents all spots where at least one pulse caused an error, either in the RM or OA signal validation. The two red bars next to it are all wrongly assigned spots. For example, if all pulses of one spot are in the no modulation category, but for at least one pulse the RM value is above threshold, it would result in a false positive. All other spots are correctly assigned by the algorithm; true negatives are represented by the blue bar, and all yellow bars are true positives. Within the true positives, a further division is possible. The first yellow bar represents all spots where the correct pulse detects the modulation. For example, if the third pulse is the first that belongs to the modulation category, the third pulse would also be the first that has a RM value above threshold. Consequently, the second yellow bar includes all spots where the one pulse before or after the correct pulse detects the modulation, and so on. The first thing to notice is the total amount of spots that generates an error during signal validation are approximately 35%. From the remaining spots, only very few are assigned wrongly by the algorithms, although the OA algorithms have slightly higher false positives and negatives. Further, the RM algorithm seems to be more accurate because the majority of the true positive spots are also detected at the correct position of the pulse train. The OA algorithm on the other hand has a greater

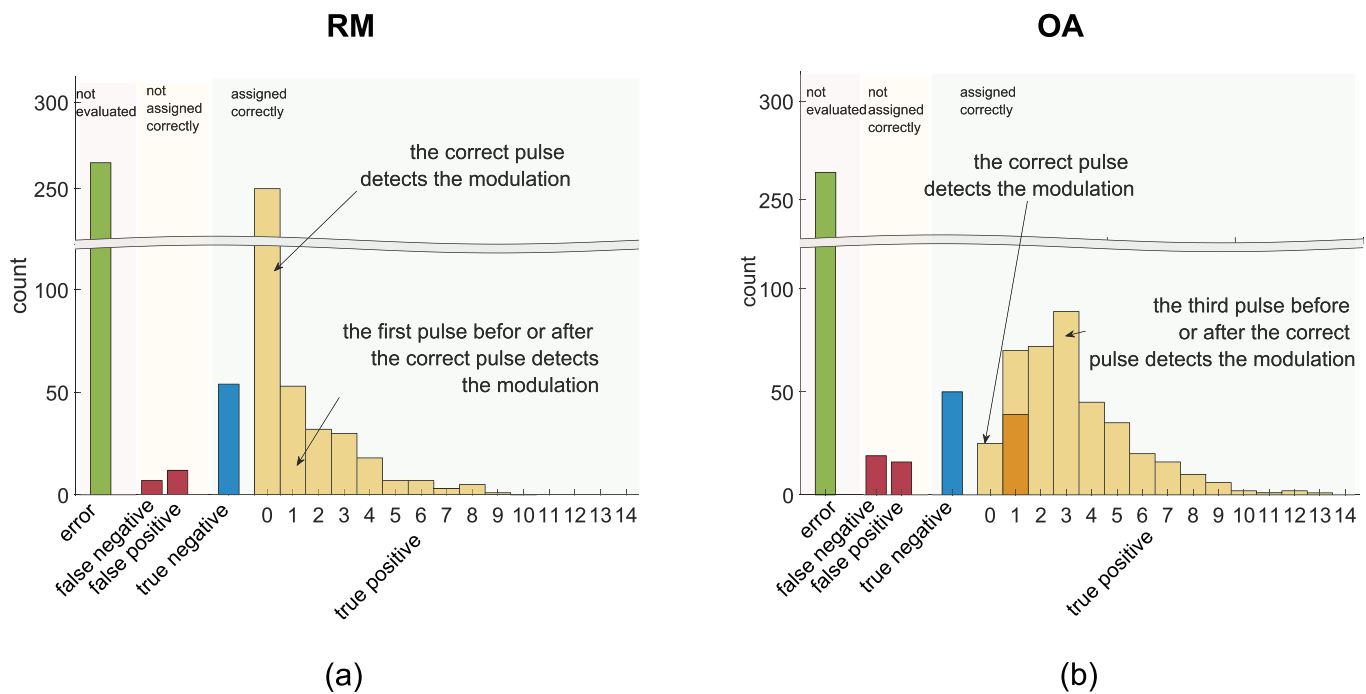


Figure 9. Histograms of all spots grouped in error, false negative, false positive, true negative, and true positive. All true positive spots are further divided in classes that represent how far from the correct pulse each algorithm detects the MB. (a) RM; (b) OA.

variation. The modulations are recognized mainly within three pulses before or after the correct pulse. In this spot wise evaluation, the RM algorithm reaches a sensitivity of 0.98 and a specificity of 0.82, and the OA algorithm 0.95 and 0.76.

Discussion

So far, no standard procedure for appropriate dosing is known for SLT because the mechanism of action is still disputed. An optimal number of pulses and pulse energies are of great interest to induce sufficient IOP reduction while avoiding side effects. MB occurring around melanin granules after temperatures exceeding the vaporization threshold could trigger the biological-induced therapeutic effects by TM cell disintegration. Therefore, we hypothesize that detecting MB could be used to guide the dosing in SLT. The goal of this study was to find MB-related signal components by two different detection methods and to develop algorithms that can potentially be used for an automatic feedback guided dosing.

SLT With Microsecond Pulses and Energy Ramp

By applying the principle of selective photothermolysis, Latina and Park⁷ showed in their initial work that pigmented cells can be targeted without coagulative damage to the surrounding tissue. They have proven the selectivity of their method using single pulses of 1 μs and 10-ns pulse duration in cultured cells.⁷ Using pulse durations of 8 μs and above, the selectivity is lost and thermal damage of the surrounding tissue was observed. For the pulse duration of 1.7 μs used in this work, no evidence was found in literature that this pulse duration is not suitable for selective cell disintegration. Although the used pulse duration is larger than the thermal relaxation time of approximately 420 ns of a single melanosome with a radius of 0.5 μm , when regarding cells, a relaxation time of 10 μs is estimated²² and different studies have shown selectivity up to pulse durations of 15 μs .^{19,23} Furthermore, with respect to thermal damage in adjacent tissue, repetitive pulses with 1.7- μs pulse duration and 100 Hz repetition rate cause selective cell killing in RPE cells in vivo.²⁴ Because the melanin density in the TM is lower compared with the RPE, it is highly unlikely that the same laser parameter will cause thermal damage in the TM. Accordingly, the pulse duration of 1.7 μs used in this study should still selectively target

pigmented cells, although the pulse duration is over 500 times larger compared with conventional SLT. The longer pulse duration holds the further advantage that the vaporization using microsecond pulses is less explosive and the bubble size is self-limiting compared with shorter pulse duration as shown by Neumann and Brinkmann.²⁵ This should improve the safety of the method with respect to collateral damage.

Instead of the conventional spot size of 400 μm , a spot size of 200 μm was used in this study. The smaller diameter does not cover the entire anteroposterior height of the TM, which might actually be an advantage. In the case of a large spot size, the outer parts of the spot can induce MBF at the iris root before MBF is induced at the TM. This would lead to an MBF-induced irradiation ceasing before the intended effect in the TM is achieved. All laser parameters of microsecond-SLT seem feasible to initiate the same mechanism of action by causing MB selectively in pigmented cells, which then cause the disruption of cell structure, triggering the actual biological pathway to initiate the therapeutic effects.^{10,17}

Optical Detection of MBs

The diode sensor data showed similar modulations as known from SRT¹⁸ when the energy is increased stepwise above a certain threshold. In SRT, these modulations are strongly correlated to cell damage and assumed to be originating from MB, being proved to be responsible for cell disintegration.²⁶ When analyzing the reflected light after microsecond-SLT, the presence of modulation suggests that MB are generated in the TM as well. It should be noted that the modulations do not start necessarily at the beginning of the pulse but most of the time further in the middle as can be seen in the first pulse of spot 2 in Figure 6a. The detection of this signal changes using the presented algorithm shows high sensitivity and specificity compared with the energy, despite its simple architecture. Using the calculated best threshold represented by the dashed line in Figure 6b, the RM values seem to be suitable to separate the modulation class from the no modulation class, although there is one wrong assigned pulse in this example set. In contrast, any energy threshold would result in no separation of the two classes. One main advantage of the presented RM algorithm is that each pulse can be analyzed on its own; the algorithm needs no reference pulse in order to prove that MBs have been achieved with the pulse. This opens the possibility of a single-pulse MB detection as well.

However, the RM detection method as presented here will likely not work in conventional 3 ns SLT systems even with a GHz detection device because bubble nucleation takes place at the end of the pulse.²⁶ However, low power probe light could be used to monitor MB after the excitation pulse. Although the presented algorithm seems to work well in this presented data set, there are plenty of other options to detect modulations. It is chosen among others because of its low complexity and good performance in SRT. The main algorithm components are similar; only algorithm parameters are adjusted for SLT. Another simple way could be the comparison of the reflected pulse with the actual excitation pulse, which could be recorded using an identical photo-diode. Analyzing the frequencies in the reflected light directly instead of filtering is another possibility.

Optoacoustical Detection of MBs

The transducer shape was chosen as a compromise between large detector area and closeness to the ultrasonic source without obstructing the light path into the eye. A half-moon shape was used to exploit the maximum area. The detector area should be large to detect large parts of the spherical emitted wave, but a big detector area could also cause interference effects and some sort of low pass filter. Experiments and simulations could be performed to fine tune the optimal transducer size. Furthermore, by finding the exact transfer function of the transducer it could be possible to correct the recorded transients. Besides the transducer shape, the angle to the ultrasonic source has an influence on the pressure amplitudes. In this first prototype, the transducer was placed orthogonal to the contact surface of the eye. The angle could be changed to optimize the transient amplitudes. However, a constant angle throughout the treatment cannot be guaranteed because the contact lens is (re-) positioned by the physician in order to visualize the chamber angle properly.

A pulse-to-pulse fluctuation of the OA transients of sequenced laser pulses was also linked to cell damage of RPE cells in SRT.²¹ This consolidates the presumption that fluctuations in SLT are caused by the formation and collapse of MB as well, because MBs cause additional pressure waves that are different compared with the pressure waves resulting from thermoelastic expansion.

A large number of transients were excluded from the evaluation because of an SNR error. But only 55% of the excluded pulses actually caused the SNR error; all others were excluded because the signal of

their reference pulse was too small compared with the noise. The mean radiant exposure of pulses causing an SNR error is 89 mJ/cm², which is far below the mean threshold for MBF of 310 mJ/cm². Therefore, the energy range in which SNR errors occur is not relevant for MBF and therefore the sensitivity of the sensor seems sufficient. Furthermore, the hardware could be adapted to select a more suitable combination of amplification and digitization in order to increase the energy range where no saturation occurs and the SNR is sufficient.

Besides the presented algorithms, different approaches were tested, such as calculating the correlation between pulses, comparing the sum of amplitude changes, or tracking the shift of peaks and zero crossings. However, with this particular data set, the presented OA algorithm performed best with respect to ROC.

Comparison of Both Methods

Both algorithms are designed to have low complexity for an easy and robust real-time MB detection. Both were able to detect signal changes most likely related to MB in porcine eyes ex vivo. For the majority of all applied pulses, a modulation in the optical signal correlates with a pulse-to-pulse fluctuation in the acoustical signal. Both algorithms have a higher combination of sensitivity and specificity than using a fixed energy threshold. The pulse wise sensitivity and specificity of the RM algorithm is higher as for the OA algorithm. But this does not necessarily mean that the OA method is less sensitive to detect MB, because the RM algorithm and the manual classification are based on the same criteria: modulations in the optical sensor signals and not on the MBF itself.

Because the labeling is based on a manual subjective classification, misinterpretations can occur especially close to the MB threshold, and it is possible that the classification of modulation and no modulation is not matching the presence of MB precisely. This wrongly labeled data could prevent the algorithms to reach higher sensitivities and specificities. This could also be the reason that in the spot wise evaluation, the RM algorithm was more accurate in predicting the correct pulse that first causes MB in each spot as shown in the histograms of Figure 9.

Using these histograms for comparison holds two disadvantages. First, the OA algorithm cannot detect a modulation on the first pulse. Thirty-nine spots had the first pulse classified as modulation, and the OA algorithm has detected them on the second pulse. They

are illustrated as the orange bar. Second, unknown pulses cannot be taken into account properly. For example, 69 (RM) and 72 (OA) spots had an unknown pulse right before the first pulse that is categorized as modulation. Thus, it is unclear which of those pulses caused MB. Therefore, all those spots could actually have been classified correctly by the algorithms.

To provide a better significance of the algorithm performance, the labeling errors could be minimized by an independent labeling by more than one person or by choosing other criteria. Besides the different accuracy in the spot wise evaluation, both algorithms reach a similar sensitivity of approximately 0.96, but the specificity differs by approximately 0.06. It should be noted that the used data set has a large class imbalance. Over 80% of the spots are categorized as modulation. Therefore, the positive predictive value (PPV = precision), and the negative predictive value (NPV) can be calculated to help interpret sensitivity and specificity. For both algorithms, the NPV is the same regime as the specificity, and the PPV is very close to the sensitivity.

To further improve the overall performance of the system, a simple combination of both algorithms could be used. In case of SLT, one would maximize the specificity to ensure a therapeutic effect. Therefore, a spot could be handled as above threshold only if both algorithms would detect MB. This would increase the spot wise total specificity to 0.96, whereas the sensitivity is 0.96 as well. In case of a more safety critical application, one would rather increase the sensitivity and cease the laser if one of the algorithms detect MB. Besides this simple combination of two thresholds, also a more sophisticated combination could be used as well as a combination of multiple algorithms at the same time. In this proof of concept study, all algorithm parameters were only adjusted manually in order reach the highest possible Youden index. An automatic parameter optimization could be implemented. Furthermore, the parameter could be optimized to reach the highest specificity. Also, both algorithms could be combined and weighted resulting in one final feedback value, optimizing the weight as well. However, an optimization procedure would be more useful in a data set from patients because all thresholds investigated in porcine eyes might not be directly transferable to humans.

A disadvantage of the RM method as reported for SRT will be less problematic in SLT. In patients with less transparent lens and cornea, the backscattered signal can become extremely low, but in SLT the light does not pass the lens, reducing this effect. The

influence of this on the OA signal quality will be even smaller because acoustic waves are detected at the sclera right above the TM. Furthermore, the OA approach can not only be used when irradiating the TM through the anterior chamber but also in the transscleral version of SLT,²⁷ it should be possible to detect MB-related transient changes.

Therapeutic Window

CBs were observed over a large energy range from 117.8 to 334 μJ . From 10 spots, a maximal ratio between the last non-MB pulse and the first CB pulse of 1.76 ± 0.24 was calculated. Because there is no information about which pulse caused the CB, it is assumed that the last pulse of each pulse train needs to be at least the first pulse causing CB. Consequently, the calculated ratio could actually be smaller.

This ratio could be useful to determine a therapeutic window. The ratio could be used as a guideline to safely increase the energy after MB detection to ensure a sufficient therapeutic effect without CB formation. Because the desired endpoint of SLT referring to the mechanism of action is not completely understood, it might be sufficient so cease the laser close above detection of MB and keep the energy as low as possible to avoid side effects as transient IOP spike or peripheral anterior synechia as suggested by Tang et al.¹⁴ Alternatively, in case a larger total energy might lead to an improved IOP reduction,¹⁵ the MB threshold could be used to add a certain percentage of energy above the MB threshold.

A therapeutic window as the ratio between CB and MBF of 1.76 is smaller than expected. Lin¹⁶ reported an energy factor of 10 between MB and CB formation, however, on single bovine melanosomes irradiated with a single nanosecond pulse at 532 nm. They also found a threshold for MBF of 55 mJ/cm^2 . However, for single porcine RPE melanosomes, thresholds of 90 and 290 mJ/cm^2 were reported by Brinkmann et al.¹⁷ for pulse durations of 8 ns and 1 μs , respectively. Thresholds increase with the pulse duration owing to heat diffusion during longer laser pulses. Also, they reported a decreased radiant exposure threshold for the damage in RPE tissue as well as decreased threshold when multiple pulses are applied because of accumulating effects.¹⁷ Thus, despite the completely different model, the different pulse duration and the fact that a pulse train is used in this study could explain the discrepancy in the ratio between micro and macro bubble formation. Furthermore, in a cluster of melanosomes, a large amount of small MB can grow together into a CB. The mean MB threshold of 310

mJ/cm² in the whole data set is in the same regime as the threshold reported by Brinkmann et al.¹⁷ with microsecond pulses. The radiant exposure typically applied in SLT ranges from 477 to 955 mJ/cm², which is in fact at least a factor 10 above the radiant exposure threshold reported for MBF using nanosecond pulses on a single melanin particle. However, the comparison of radiant exposure is difficult due to the uncertainty in determining the correct spot size, and it should be noted again that these experiments were performed in porcine eyes and therapeutic windows found here might not directly apply to human eyes. Also, the number of spots from which the ratio between MB and CB is calculated here might be too small to directly draw conclusions of an optimal therapeutic window.

Toward a Feedback System

Clinical trials are needed using a ramp of microsecond pulses to investigate what kind of cell damage is needed to ensure a sufficient IOP reduction. In the first stage, it is necessary to determine if small MB cause adequate cell disintegration to trigger the IOP reduction or if larger bubbles are needed. Consequently, an energy threshold correlated to the threshold of MBF needs to be found first. This threshold, whether it is close to the formation of MB or CB, can then be used in an automatic feedback loop controlling the laser irradiation.

The presented algorithms are real-time capable, detect MBF accurately and could therefore be used in a feedback loop controlling the laser irradiation. The pulse ramp could, for example, be automatically ceased upon MB detection with one or both detection methods. Even if the better IOP reduction is reached with energies closer to the threshold of CB formation, this system could still be extremely useful to apply adequate energy that is effective and safe. The integration of both feedback techniques into a SLT laser system should cause no major challenges. However, the high number of error pulses found with the system investigated here point out that the amplification and digitization need to be chosen carefully.

Conclusions

We demonstrated accurate detection of MBF in the TM of porcine eye globes ex vivo with an SRT laser system that is under investigation for SLT. Micro and macro bubbles could be achieved with microsecond pulses used with the presented system with an average threshold radiant exposure of 310 ±

137 mJ/cm², which is smaller than the radiant exposure typically used in SLT. With a combination of both an optical and acoustical evaluation, a sensitivity and specificity of 0.96 to detect MBF can be reached with an RM threshold of 2.67E-6 and an OA threshold of 108.57, respectively, when evaluating spot wise. The RM algorithm developed here seems to be more sensitive to detect MB and more accurate in detecting the correct pulse that first causes MB.

In case that the therapeutically demanded IOP reduction is already achieved with MB, which needs to be proven clinically, the presented methods can be used in a feedback loop controlling the laser irradiation; that is, the pulse ramp can be automatically ceased upon detection of MBF. Even if the first formation of MBs prove not to be the ideal endpoint, the onset of them could be used as guidance to set an adequate energy. A maximal ratio between MB and CB formation of 1.76 ± 0.24 was found, which could be used to reliably set an energy close to the threshold for CB formation. The presented algorithms on their own are not able to differentiate between MB and CB, because CBs seem not to cause any further signal changes. CBs could be monitored by light reflection using the pilot light, because CBs are lasting for seconds. Nonetheless, an automatic detection of MBs could unburden the clinicians from dosing during SLT and can help to reduce overtreatment and undertreatment.

Acknowledgments

This work was supported by the World Class 300 Project (S2340708) of the SMBA (Small and Medium Business Administration), Republic of Korea.

Disclosure: **K. Bliedtner**, None; **E. Seifert**, None; **R. Brinkmann**, optical detection (P), laser control (P)

References

1. National Institute for Health and Care Excellence. Glaucoma: diagnosis and management (NICE guideline [NG81]) (2017). Available at: [nice.org.uk/guidance/ng81](https://www.nice.org.uk/guidance/ng81). Accessed April 10, 2019.
2. DiMatteo MR. Variations in patients' adherence to medical recommendations: a quantitative

- review of 50 years of research. *Med Care*. 2004;42:200–209.
3. Robin AL, Novack GD, Covert DW, Crockett RS, Marcic TS. Adherence in glaucoma: objective measurements of once-daily and adjunctive medication use. *Am J Ophthalmol*. 2007;144:533–540.
 4. Stone JL, Robin AL, Novack GD, Covert DW, Cagle GD. An objective evaluation of eyedrop instillation in patients with glaucoma. *Arch Ophthalmol*. 2009;127:732–736.
 5. Wise JB, Witter SL. Argon laser therapy for open-angle glaucoma: a pilot study. *Arch Ophthalmol*. 1979;97:319–322.
 6. Wise JB. Long-term control of adult open angle glaucoma by argon laser treatment. *Ophthalmology*. 1981;88:197–202.
 7. Latina MA, Park C. Selective targeting of trabecular meshwork cells: in vitro studies of pulsed and CW laser interactions. *Exp Eye Res*. 1995;60:359–371.
 8. Latina MA, Sibayan SA, Shin DH, Noecker RJ, Marcellino G. Q-switched 532-nm nd: YAG laser trabeculoplasty (selective laser trabeculoplasty): a multicenter, pilot, clinical study. *Ophthalmology*. 1998;105:2082–2090.
 9. Damji KF, Bovell AM, Hodge WG, et al. Selective laser trabeculoplasty versus argon laser trabeculoplasty: results from a 1-year randomised clinical trial. *Br J Ophthalmol*. 2006;90:1490–1494.
 10. Kramer TR, Noecker RJ. Comparison of the morphologic changes after selective laser trabeculoplasty and argon laser trabeculoplasty in human eye bank eyes. *Ophthalmology*. 2001;108:773–779.
 11. Kagan DB, Gorfinkel NS, Hutnik CM. Mechanisms of selective laser trabeculoplasty: a review. *Clin Exp Ophthalmol*. 2014;42:675–681.
 12. Samples JR, Singh K, Lin SC, et al. Laser trabeculoplasty for open-angle glaucoma: a report by the American Academy of Ophthalmology. *Ophthalmology*. 2011;118:2296–2302.
 13. Nagar M, Ogunyomade A, O'brart DPS, Howes F, Marshall J. A randomised, prospective study comparing selective laser trabeculoplasty with latanoprost for the control of intraocular pressure in ocular hypertension and open angle glaucoma. *Br J Ophthalmol*. 2005;89:1413–1417.
 14. Tang M, Fu Y, Fu M, et al. The efficacy of low-energy selective laser trabeculoplasty. *Ophthalmic Surg Lasers*. 2011;42:59–63.
 15. Lee JW, Wong MO, Liu CC, Lai JS. Optimal selective laser trabeculoplasty energy for maximal intraocular pressure reduction in open-angle glaucoma. *J Glaucoma*. 2015;24:e128–e131.
 16. Lin CP. Selective absorption by melanin granules and selective cell targeting. In: Fankhauser F, Kwasniewska S, eds. *Lasers in Ophthalmology—Basic, Diagnostic and Surgical Aspects*. Amsterdam, the Netherlands: Kugler Publications, The Hague; 2003:91–98.
 17. Brinkmann R, Hüttmann G, Rögner J, Roeder J, Birngruber R, Lin CP. Origin of retinal pigment epithelium cell damage by pulsed laser irradiance in the nanosecond to microsecond time regimen. *Lasers Surg Med*. 2000;27:451–464.
 18. Seifert E, Tode J, Pielen A, et al. Selective retina therapy: toward an optically controlled automatic dosing. *J Biomed Opt*. 2018;23:115002.
 19. Alt C, Framme C, Schnell S, Lee H, Brinkmann R, Lin CP. Selective targeting of the retinal pigment epithelium using an acousto-optic laser scanner. *J Biomed Opt*. 2005;10:064014.
 20. Zbinden S, Kucur ŞS, Steiner P, Wolf S, Sznitman R. Automatic assessment of time-resolved OCT images for selective retina therapy. *Int J Comput Assist Radiol Surg*. 2016;11:863–871.
 21. Schuele G, Elsner H, Framme C, Roeder J, Birngruber R, Brinkmann R. Optoacoustic real-time dosimetry for selective retina treatment. *J Biomed Opt*. 2005;10:064022.
 22. Brinkmann R, Roeder J, Birngruber R. Selective retina therapy (SRT): a review on methods, techniques, preclinical and first clinical results. *Bull Soc Belge Ophthalmol*. 2006;302:51–69.
 23. Schuele G, Rumohr M, Huettmann G, Brinkmann R. RPR damage thresholds and mechanisms for laser exposure in the microsecond-to-millisecond time regimen. *Invest Ophthalmol Vis Sci*. 2005;46:714–719.
 24. Park YG, Seifert E, Roh YJ, Theisen-Kunde D, Kang S, Brinkmann R. Tissue response of selective retina therapy by means of a feedback-controlled energy ramping mode. *Clin Exp Ophthalmol*. 2014;42:846–855.
 25. Neumann J, Brinkmann R. Self-limited growth of laser-induced vapor bubbles around single micro-absorbers. *Appl Phys Lett*. 2008;93:033901.
 26. Neumann J, Brinkmann R. Cell disintegration by laser-induced transient microbubbles and its simultaneous monitoring by interferometry. *J Biomed Opt*. 2006;11:041112.
 27. Geffen N, Ofir S, Belkin A, et al. Transscleral selective laser trabeculoplasty without a gonioscopy lens. *J Glaucoma*. 2017;26:201–207.